

Mercury Removal from Contaminated Water by Wood-Based Biochar Depends on Natural Organic Matter and Ionic Composition

Sampriti Chaudhuri, Gabriel Sigmund, Sharon E. Bone, Naresh Kumar, and Thilo Hofmann*



Cite This: *Environ. Sci. Technol.* 2022, 56, 11354–11362



Read Online

ACCESS |

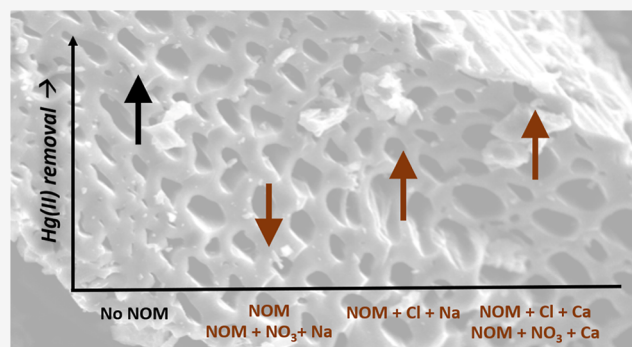
Metrics & More

Article Recommendations

Supporting Information

ABSTRACT: Biochars can remove potentially toxic elements, such as inorganic mercury [Hg(II)] from contaminated waters. However, their performance in complex water matrices is rarely investigated, and the combined roles of natural organic matter (NOM) and ionic composition in the removal of Hg(II) by biochar remain unclear. Here, we investigate the influence of NOM and major ions such as chloride (Cl^-), nitrate (NO_3^-), calcium (Ca^{2+}), and sodium (Na^+) on Hg(II) removal by a wood-based biochar (SWP700). Multiple sorption sites containing sulfur (S) were located within the porous SWP700. In the absence of NOM, Hg(II) removal was driven by these sites. Ca^{2+} bridging was important in enhancing removal of negatively charged Hg(II)-chloro complexes. In the presence of NOM, formation of soluble Hg-NOM complexes (as seen from speciation calculations), which have limited access to biochar pores, suppressed Hg(II) removal, but Cl^- and Ca^{2+} could still facilitate it. The ability of Ca^{2+} to aggregate NOM, including Hg-NOM complexes, promoted Hg(II) removal from the dissolved fraction ($<0.45 \mu\text{m}$). Hg(II) removal in the presence of Cl^- followed a stepwise mechanism. Weakly bound oxygen functional groups in NOM were outcompeted by Cl^- , forming smaller-sized Hg(II)-chloro complexes, which could access additional intraparticle sorption sites. Therein, Cl^- was outcompeted by S, which finally immobilized Hg(II) in SWP700 as confirmed by extended X-ray absorption fine structure spectroscopy. We conclude that in NOM containing oxic waters, with relatively high molar ratios of Cl^- : NOM and Ca^{2+} : NOM, Hg(II) removal can still be effective with SWP700.

KEYWORDS: sorption, speciation, industrial effluents, porosity, cation bridge, ligand exchange, extended X-ray absorption spectroscopy, reduction



INTRODUCTION

The prevalence and acute toxicity of mercury (Hg(II)) have been well documented.¹ In 2013, the Minamata Convention recognized the immediate need to reduce the use of Hg(II) and Hg emissions globally.² Despite efforts to limit Hg(II) waste, anthropogenic activities generating Hg(II)-containing wastewaters continue in many developing nations. For example, effluents from many gold mining areas,³ coal power plants,⁴ biomedical,⁵ paper and pulp industries,⁶ and even groundwater in some historically contaminated sites⁷ still continue to report high Hg(II) concentrations ranging between 0.75 and 10 μM . To treat such contaminated waters, novel materials are being developed, including polymers,⁸ functionalized clays,⁹ carbonaceous materials,¹⁰ and composites thereof.¹¹ Although these sorbents are widely investigated, their large-scale application may be economically challenging in low-income countries. The use of a low-cost carbonaceous sorbent such as biochar may provide an alternative to treat Hg(II)-contaminated waters. Biochar can be produced from agricultural and wood waste, which can support sustainable remediation approaches.

Studies report efficient removal of Hg(II) (as ionic Hg^{2+}) using biochar due to its high porosity, surface functional groups that complex with Hg(II), and its highly aromatic structure enabling Hg- π binding.^{12,13} However, Hg^{2+} is a rare form of Hg(II) in water and occurs only under strongly acidic environments and in the absence of complexing ligands.¹⁴ In contaminated waters, Hg(II) removal efficiency in sulfide-free conditions will be dependent on pH, natural organic matter (NOM) content, and ions such as chloride (Cl^-), which determine Hg(II) speciation as HgCl_2 , HgCl_3^{1-} , HgCl_4^{2-} , HgClOH , or Hg-NOM complexes.

NOM, being ubiquitous in contaminated waters,¹⁵ may inhibit Hg(II) removal due to the formation of aqueous Hg-NOM complexes and competition over sorption sites.^{16,17}

Received: March 4, 2022

Revised: July 22, 2022

Accepted: July 22, 2022

Published: August 4, 2022



Sorbed NOM can also offer new sorption sites and increase Hg(II) removal from aqueous solutions.¹⁸ Cl^- is a major anion in many natural and anthropogenic waters¹⁹ and strongly complexes with Hg(II) as Hg(II)-chloro complexes.²⁰ Higher Cl^- concentrations forming stable dissolved HgCl_2 can inhibit Hg(II) immobilization.²¹ The ratios of NOM/Hg(II), $\text{Cl}^-/\text{Hg(II)}$, and NOM/Cl^- determine Hg(II) distribution as Hg-NOM or Hg(II)-chloro complexes. The presence of other cations induces changes in NOM by increasing their hydrophobicity through inner and outer sphere complexation.²² This may affect the complexation behavior of Hg(II) with NOM and its removal by sorbents.

Water chemistry also influences the biochar surface: alkaline pH increases its negative surface charge,²³ NOM can block small pores and sorb onto the surface,²⁴ and cations in solution can decrease the negative surface charge of biochar.²⁵ Ternary interactions between biochar, Hg(II), and NOM, as well as coexisting ions are expected to impact Hg(II) removal by biochar. These intertwined mechanisms are largely under-investigated. The influence of complex water chemistry on Hg(II) immobilization by novel carbonaceous sorbents such as biochar is crucial to understand prior to full-scale application.

To address this knowledge gap, we aim to investigate the influence of major anions, cations, and NOM on Hg(II) removal by a standardized wood-based biochar under sulfide-free conditions. Complex systems are represented by different coexisting background ions with peat soil-extracted NOM. We investigate the interdependence of these parameters on Hg(II) removal from contaminated waters having high Hg(II) concentrations typical of wastewater effluents and streams. Laboratory batch experiments are combined with X-ray absorption spectroscopy to provide mechanistic insights into the atomic coordination environments of immobilized Hg(II). Although NOM may decrease Hg(II) removal, we hypothesize that the existence of Cl^- and Ca^{2+} in such systems can counter this effect. Our study advances the applicability of biochars in removing Hg(II) from contaminated waters with different background complexities.

MATERIALS AND METHODS

Preparation of NOM Extract. NOM was extracted from bulk Pahokee Peat material (IHSS-2BS103P) because it is a well-investigated representative of the complex NOM encountered in field scenarios. NOM was extracted via an alkaline extraction process, detailed in Section 1 of the [Supporting Information](#). This extract was quantified for operationally defined ($<0.45 \mu\text{m}$) dissolved organic carbon (DOC) on a TOC analyzer (TOC-L_{CPH/CPN}, Shimadzu, Japan), measuring nonpurgeable organic carbon, and used as stock for all sorption experiments. A portion of this extract was lyophilized to determine the total C and S contents using an elemental analyzer (Elementar VarioMacro, Elementar Analysensysteme GmbH, Germany). NOM was calculated to be 2.31 times the DOC concentration in mg L^{-1} .

Background Solutions. Deionized water derived from an Elga PURELAB Chorus 3 water purification unit (ELGA LabWater, UK) was used to prepare all solutions. Solutions with different background electrolytes were produced from 1M stock solutions of sodium chloride (NaCl), sodium nitrate (NaNO_3), calcium chloride dihydrate ($\text{CaCl}_2 \cdot 2\text{H}_2\text{O}$), and calcium nitrate tetrahydrate [$\text{Ca}(\text{NO}_3)_2 \cdot 4\text{H}_2\text{O}$]. Hg(II) stock solution was prepared by dissolving mercuric chloride (HgCl_2)

in water. All salts were of analytical grade and purchased from Merck, Germany.

Hg-NOM intermediate working solutions were diluted from stock solutions of Hg(II) and NOM and pre-equilibrated in the dark for 72 h to allow Hg(II) to complex with available binding sites in NOM. Hg(II) reacts with strong binding sites containing S within a few hours.²⁶ Since we investigated scenarios of higher Hg(II) contamination, such as waste water streams and industrial effluents, a longer reaction time was allowed to facilitate Hg(II) complexation with O containing sites. Oxidic conditions and a preliminary experiment with these solutions ensured that NOM caused minor formation of Hg(0), that is, $93 \pm 3\%$ of Hg(II) was recovered from the aqueous phase and the bottle walls, after purging with N_2 for 30 min.

The solutions used in the sorption experiments were composed of mixtures of equal volumes of Hg(II) intermediate solution (Hg-NOM or NOM-free) and electrolyte solution with the final Hg(II) concentration kept at $2.5 \mu\text{M}$. The pH was allowed to equilibrate to a value buffered by the biochar at 6.9 ± 0.6 (mean \pm SD). Owing to the range of NOM concentrations in contaminated waters,²⁷ we conducted experiments using 0 mg L^{-1} NOM, 4.6 mg L^{-1} NOM, and 46.2 mg L^{-1} NOM with extensive investigation at 46.2 mg L^{-1} where significant effects were discernible. To study the effects of individual ions and their concentrations, we kept the concentration of the respective anionic/cationic counterpart constant. Maximum Ca^{2+} concentration was kept at 20 mM since higher concentrations typically do not occur²⁷ and would have aggregated all NOM, reducing the reliability of our results.

A separate set of experiments with NaCl solutions were conducted at a lower pH of 5.0 using 10 mM 2-(*N*-morpholino) ethanesulfonic acid (MES) buffer purchased from Alfa Aesar, Germany. MES buffer has previously been used in studies with NOM,²⁸ Hg(II),²⁹ and with solid phases including biochar³⁰ and soil.³¹

Windermere Humic Aqueous Model VI Speciation of Background Solutions. Approximate estimations of Hg(II) speciation in each background solution were made using the Windermere Humic Aqueous Model (WHAM VI), which assumes a series of discrete site pK_a values for metal binding with humic substances. WHAM VI combines the inorganic speciation code WHAM with a submodel of humic ion binding model VI. Oftentimes, metal binding by NOM can be overestimated if the true proportion of NOM available for metal binding is not used.³² Therefore, we assumed that the binding sites for Hg(II) exist predominantly in the hydrophobic fraction of NOM (humic and fulvic acids). For NOM-containing systems, we updated the model with lowered intrinsic binding constants of Hg(II) with humic and fulvic acids (assuming these are only carboxylic and phenolic groups) and separate thermodynamic constants for reactive thiol groups. Further details, including the assumptions made, the equations and constants used, and calculations, are provided in Section 2 of the [Supporting Information](#).

Sorption Experiments. The majority of biochars reported in the literature are produced within $500\text{--}800 \text{ }^\circ\text{C}$.³³ A woody biochar produced from soft wood pellets (5:95 pine/spruce) pyrolyzed at $700 \text{ }^\circ\text{C}$ (SWP700) was purchased from UK Biochar Research Center (UKBRC, Edinburg, UK). We chose this relatively high-temperature biochar based on its good performance observed in preliminary sorption tests among a

suite of 10 standardized biochars (data not shown). Higher pyrolysis temperatures may result in the loss of C-bound S groups, which are the principal drivers for Hg(II) removal.³⁴ Further details on the biochar production and characterization are provided in Section 4 of the [Supporting Information](#).

For each experiment, 25 mg of crushed SWP700 (<0.25 mm) was equilibrated in the dark at 125 rpm with 25 mL of background solutions containing Hg(II). SWP700 only leached low levels of NOM (2 ± 1.2 mg C L⁻¹) and inorganic ions (<0.01 mM of anions and cations measured by ion chromatography and inductively coupled plasma optical emission spectroscopy, respectively) and caused negligible changes to water chemistry during experimentation. After 48 h, the tubes were centrifuged at 1000 g (Sorvall LYNX 6000, Thermo Fischer, USA) and the solutions were filtered through 0.45 μ m cellulose acetate filters (Sartorius, Germany). The filtered supernatants were analyzed for total Hg(II) following US EPA method 1631 using cold vapor atomic fluorescence spectroscopy (CVAFS, DMA 80-L, Milestone, Italy), and sorption coefficients (K_d) were calculated. Details on the measurement and calculations are provided in Sections 5 and 6 of the [Supporting Information](#), respectively. Control experiments without biochar were used to check for the aqueous phase recovery of Hg(II) in background solutions. Loss to filter material was monitored and found to be negligible. Details for both are provided in Section 3 of the [Supporting Information](#). Tukey's post hoc test was applied after running a one-way ANOVA on the K_d values to examine the differences ($p < 0.05$) between pairs of means. In cases of skewed K_d observations, because of a K_d value larger than the rest by 2 orders of magnitude, we ran the tests excluding that value.

The zeta (ζ) potential of the biochar suspensions, which correlates with the surface charge, was calculated by measuring the electrophoretic mobility using a Litesizer 500 (Anton Paar GmbH, Austria) system. Section 7 of the [Supporting Information](#) provides further details of the measurements. The DOC in solutions with high NOM (46.2 mg L⁻¹ of NOM) was monitored after sorption experiments using a TOC analyzer (TOC-L_{CPH/CPN}, Shimadzu, Japan).

Solid-Phase Analysis. Four selected scenarios at the highest investigated NOM (46.2 mg L⁻¹) and electrolyte concentrations [100 mM NaCl, 100 mM NaNO₃, 20 mM CaCl₂, and 20 mM Ca(NO₃)₂] were scaled up 10-fold (250 mg in 250 mL) at the same Hg(II) concentration for solid-phase analysis. At the end of sorption experiments, the samples were filtered under vacuum. To wash out remaining salts, the solids were resuspended and washed with deionized water multiple times. Last, the samples were dried in a desiccator under vacuum. The final loading of Hg(II) on the biochars was >250 mg kg⁻¹ for all, except the NaNO₃ system (<50 mg kg⁻¹).

Hg solid-phase speciation [samples with Hg(II) > 250 mg kg⁻¹] was determined using Hg L_{III}-edge extended X-ray absorption fine structure (EXAFS) spectroscopy conducted at beamline 7-2 at the Stanford Synchrotron Radiation Light-source, which is equipped with a Si(111) double-crystal monochromator. Two-dimensional micro-X-ray fluorescence (μ -XRF) mapping using a 25 μ m diameter focused beam was initially used to find associations between elements including Hg, Cl, and S. A representative 25 μ m spot from each sample was selected for Hg L_{III}-edge EXAFS spectroscopy. All data processing and fitting of the EXAFS spectra were performed using Athena and Artemis,³⁵ respectively. A detailed

description of the μ -XRF mapping, selection of EXAFS points, data processing, and fitting can be found in Sections 10 and 11 of the [Supporting Information](#).

X-ray diffractograms (XRD) were obtained for the vacuum-dried samples to rule out crystalline-phase precipitation during the experiment [for instance reduction of Hg(II) to Hg₂Cl₂]. Energy-dispersive X-ray spectroscopy (EDS) was used to detect significant quantities of elements such as Cl, Ca, and Na on the biochar surface after sorption. Details for both measurements are provided in Section 9 of the [Supporting Information](#).

RESULTS AND DISCUSSION

Microporous SWP700 Removes Hg(II) by Multiple Mechanisms. SWP700 is a woody biochar produced at 700 °C. Due to the high pyrolysis temperature, SWP700 is highly carbonized with 90.0% C, 6.1% O, and a specific surface area of 184.4 m² g⁻¹ (Table S4).

High pyrolytic temperature in biochars generally translates to high pore volume and water holding capacity.³⁶ SEM imaging of SWP700 shows a highly porous framework consisting of macro- (Figures 1 and S2), meso-, and

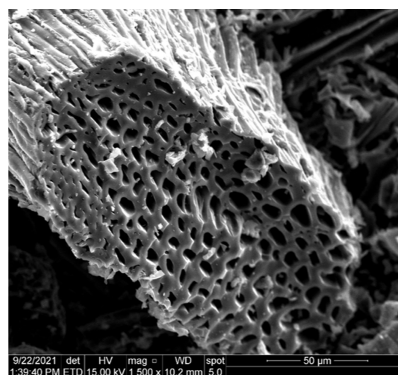
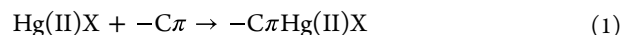


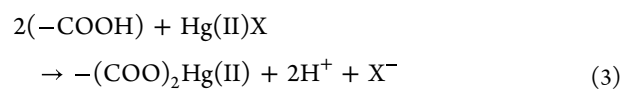
Figure 1. Scanning electron micrograph of SWP700 biochar particle (magnification 1500 \times).

micropores, which could be penetrated by water transporting dissolved Hg(II) species. Recent studies using the same biochar show that 95% of the total porosity in SWP700 corresponds to a pore width of <3 μ m,³⁷ with 1.4 and 7.8% consisting of micro- (<2 nm) and mesopores (2–50 nm), respectively.³⁸ Hg(II) can be immobilized at sites on the external surface and within this porous framework.

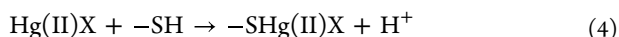
The measured low H/C molar ratio of 0.22 indicates a highly condensed aromatic structure that makes SWP700 more aromatic than 92.5% of biochars screened in a recent meta-analysis.³³ The high aromaticity of SWP700 can cause its π electron system to substantially contribute to Hg(II) immobilization (eq 1).^{12,13}



At the studied pH of 6.9 ± 0.6 , carboxylic moieties on SWP700 are deprotonated and can also participate in complexation reactions (eqs 2 and 3).



Binding constants ($\log K$) of Hg(II) with carboxylic moieties are between 7.3 and 11, while those for Hg(II) with S moieties (e.g., thiols) are higher in the range of 21–47.⁴⁹ Binding with S moieties is thus expected to govern Hg(II)-biochar interactions as long as such sites are available.³⁹ With a total S content of 0.18% (Table S4) and assuming reactive S of 75% for a high-temperature woody biochar,⁴⁰ 17 mM S binding sites on SWP700 ($S_{\text{reactive,SWP700}}$) were available per mM Hg(II) at the experimental solid-to-liquid ratio. Thus, S binding sites were in excess of Hg(II) and were expected to drive Hg(II) removal from the aqueous phase (eq 4).



Coexistence of Ca^{2+} and Cl^- Influences Hg(II) Removal in the Absence of NOM. Figure 2a shows the different K_d values observed under different water chemistry conditions in NOM-free systems. SWP700 was an effective sorbent for Hg(II), with K_d ranging between 5500 and 56 000 L kg^{-1} . Other studies using similar unmodified biochars and activated carbons made from coconut shell,¹³ bagasse,¹³ pine,¹⁷ banana peel,⁴¹ and corn straw⁴² report similar K_d values ranging between 5000 and 25 000 L kg^{-1} . SWP700 was also more effective than two activated carbons we previously tested—a wood-based activated carbon and a commercial powdered activated carbon NORIT Super SAE—which had K_d values of <1000 and 20 000 L kg^{-1} , respectively (data not shown).

WHAM calculations (Figure 2b) indicate that in deionized water and solutions containing either NaNO_3 or $\text{Ca}(\text{NO}_3)_2$,

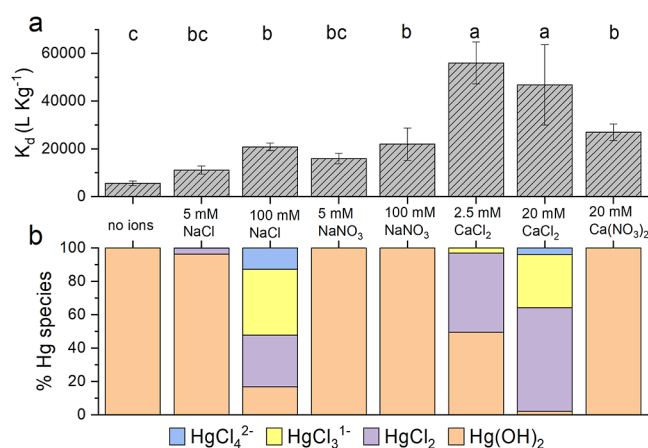


Figure 2. Hg(II) removal by SWP700 without NOM in the presence of different background ions. (a) Sorption coefficients (K_d) of Hg(II), with (b) corresponding Hg(II) speciation in the background solution modeled using the geochemical code WHAM. pH values used in modeling were derived from measurements at the end of the sorption batch experiments, which are shown in Figure S3 of the Supporting Information. Error bars represent standard deviation of at least triplicate measurements. For pairwise comparison of means, the Tukey's post hoc test was used after running one-way ANOVA ($p < 0.05$).

Hg(II) exists in the hydroxyl form [as $\text{Hg}(\text{OH})_2$]. With the addition of 5 mM NaCl, HgCl_2 is formed and additional Cl^- leads to the dominance of negatively charged species (HgCl_4^{2-} and HgCl_3^{-}). With the exception of CaCl_2 (K_d between 46 795 to 56 000 L kg^{-1}), significant differences in Hg(II) removal by SWP700 were absent when comparing various ionic compositions (Figure 2a). Lower pH values were observed

in SWP700 suspensions with Ca^{2+} (between 6.2 and 6.8) compared to Na^+ (between 7.5 and 8.0) (Figure S3). This drop in pH can be linked to competition of Ca^{2+} with protons for proton binding sites in SWP700. The electro-kinetic potential (ζ -potential) is often used as a proxy for particle surface charge. Substantially decreased negative ζ -potentials of SWP700 indicate a higher degree of charge screening by Ca^{2+} (−11 to −21 mV) compared to Na^+ (−39 to −53.5 mV). In CaCl_2 systems, this facilitates the sorption of negatively charged Hg(II)-chloro complexes, and cation bridging might have further enhanced this removal.⁴³ Furthermore, we observed distinctively lower Hg(II) removal ($p < 0.05$) in $\text{Ca}(\text{NO}_3)_2$ systems where charged Hg(II)-chloro species were absent. The speciation of Hg(II) as charged Hg(II)-chloro molecules and the coexistence of divalent cations are important to understand enhanced Hg(II) removal in systems without NOM.

Increasing NOM Concentrations Decreases Hg(II) Removal. We observed a trend of decreasing Hg(II) removal with increasing NOM concentrations (Figure 3a). Presence of

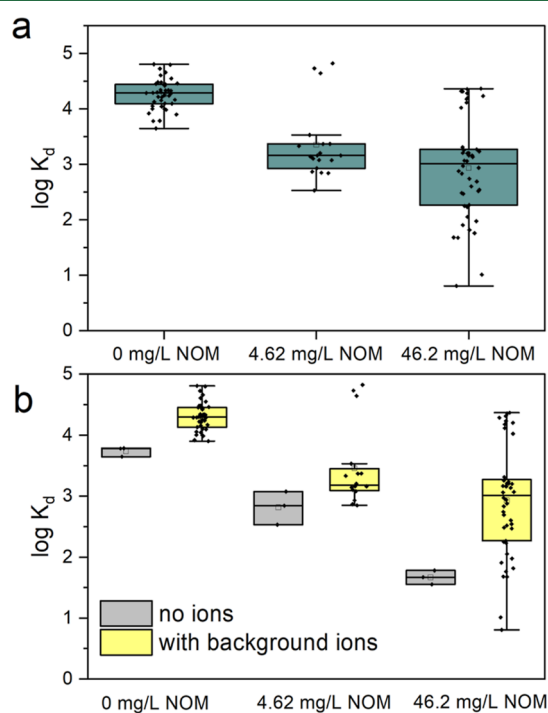


Figure 3. Trends showing Hg(II) removal in the presence of NOM. (a) Box plots of logarithmic sorption coefficients across different NOM levels and (b) comparison of box plots of logarithmic sorption coefficients across NOM levels without and with background ions (5 mM Na^+ + 5 mM Cl^- , 100 mM Na^+ + 100 mM Cl^- , 2.5 mM Ca^{2+} + 5 mM Cl^- , 20 mM Ca^{2+} + 40 mM Cl^- , 2.5 mM Ca^{2+} + 5 mM and NO_3^- , and 20 mM Ca^{2+} + 40 mM NO_3^-).

NOM leads to the formation of thermodynamically stable Hg-NOM species. Humic and fulvic acids in Pahokee Peat are large NOM molecules and have relatively high molecular weights (weight-averaged molecular weights of 15.4 kDa and 6.9 kDa, respectively).⁴⁴ Such large NOM molecules complexed to Hg(II) would have limited access to internally located pores in SWP700. SWP700 contains abundant graphitic microstructures (Figure 1) with potential Hg(II) sorption sites. Feng et al.⁴⁵ showed that at pyrolysis temperatures between 300 and 900 °C, S distribution extends

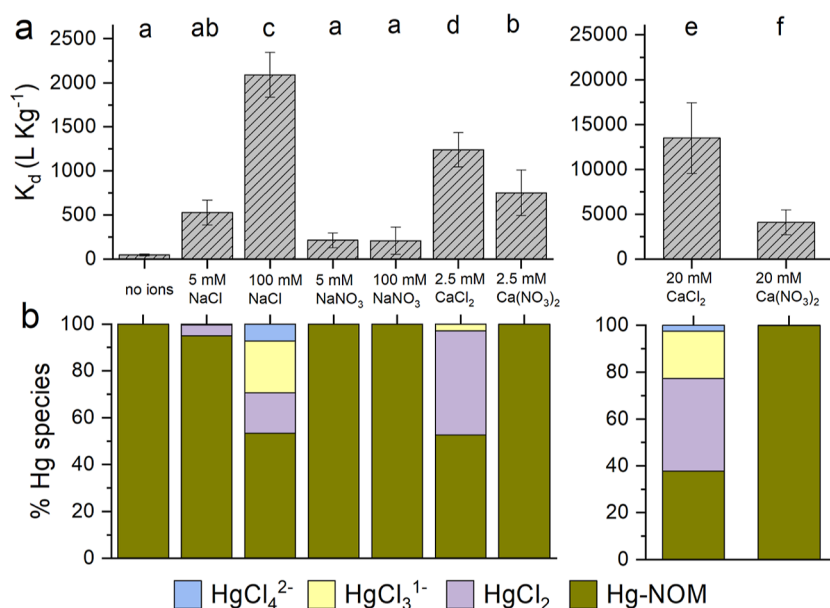


Figure 4. Hg(II) removal by SWP700 in the presence of NOM and different background ions. (a) Sorption coefficients (K_d) of Hg(II) to SWP700 with 20 mg C L⁻¹ of NOM (or, 46.2 mg L⁻¹ of NOM) and (b) corresponding Hg(II) speciation in the background solution. pH values used in modeling were derived from measurements at the end of the sorption batch experiments, which are shown in Figure S3 of the Supporting Information. Error bars represent standard deviation of at least triplicate measurements. For pairwise comparison of means, the Tukey's post hoc test was used after running one-way ANOVA ($p < 0.05$).

to locations within this porous network in woody biochars. S sites within SWP700 may thus be crucial for Hg(II) removal in our study. In addition, NOM molecules can block pores and compete for sorption sites by attaching onto the SWP700's surface via π - π electron donor-acceptor interactions and hydrophobic effects.⁴⁶ Thus, NOM may have inhibited Hg(II) removal by SWP700 via these two complementary processes.

In deionized water, the logarithmic K_d at 46.2 mg L⁻¹ of NOM was 1.6 (Figure 3b). However, we observed that the presence of other background ions (Cl⁻, NO₃⁻, Ca²⁺, and Na⁺) caused large variations in K_d spanning more than 3 orders of magnitude (log K_d between 0.8 and 4.4). This suggests that in the presence of NOM, Hg(II) removal is also affected by ionic composition.

Ionic Composition Determined Hg(II) Removal in the Presence of NOM. WHAM VI estimated that with 46.2 mg L⁻¹ of NOM, Hg-NOM species become abundant in all solutions (Figure 4b). At Hg/NOM ratios ≤ 1 μ g Hg/mg NOM, Hg(II) is solely associated with strong binding sites in NOM such as reactive S or thiolate groups.⁴⁷ In this study, using a Hg/NOM ratio of 10.8 μ g Hg/mg NOM, Hg(II) was also bound to weaker O containing sites in NOM. The moles of reactive S in NOM ($S_{\text{NOM, reactive}}$) were calculated by eq 5. Based on the total C and S measurements of the lyophilized NOM extract, NOM is 2.31 times the amount of DOC in mg L⁻¹ in solution and S_{total} is 0.92%. Since Pahokee Peat is an agricultural peat soil from the marshes in the Florida Everglades, we used literature-based values specific to this region for S_{reduced} and S_{reactive} which were taken to be as 50 and 2%, respectively.⁴⁷⁻⁴⁹

$$S_{\text{NOM, reactive}} = \frac{\text{NOM} \times S_{\text{total}} \times S_{\text{reduced}} \times S_{\text{reactive}}}{\text{Molecular weight S}} \quad (5)$$

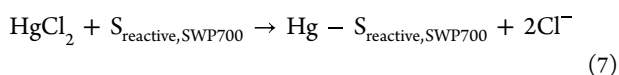
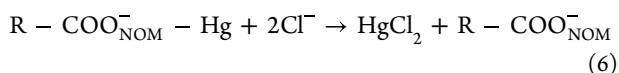
The Hg(II)/ $S_{\text{NOM, reactive}}$ molar ratio was calculated to be $\sim 19:1$ in all solutions containing 46.2 mg L⁻¹ NOM. Hg(II) was therefore in excess of the reactive S in NOM. Reactive S

sites were saturated, and a large fraction of the modeled Hg-NOM complexes consisted of Hg(II) bound to carboxyl and phenolic groups in NOM. Even when considering an upper limit of 30% for S_{reactive} ⁴⁹ we calculated the Hg(II)/ $S_{\text{NOM, reactive}}$ molar ratio to be 1.25:1.

We observed that Hg(II) removal increased with increasing NaCl concentration in the presence of NOM, like NOM-free systems (Figure 4a). The speciation of Hg(II) in 100 mM NaCl comprised of Hg(II)-chloro and Hg-NOM complexes. Na⁺ can shield negative charges over SWP700 to allow negatively charged species (HgCl₃¹⁻/HgCl₄²⁻) to sorb. A slight decrease in negative ζ potential from -32 to -25 mV was observed on increasing the NaCl concentration from 5 mM to 100 mM. However, this is not significant enough to have caused increased Hg(II) removal in the 100 mM NaCl system. Na⁺ can also interact with NOM, and this could increase the hydrophobicity of NOM, causing sorption of NOM and NOM complexed to Hg(II). However, we observed only a minor NOM loss of <5% at the end of the experiments, suggesting that this mechanism was not dominating (Figure S4). Loss of Hg(II) as volatile Hg(0) was also ruled out since experiments were conducted in oxic conditions and contained Cl⁻.^{50,51} Observed XRD indicated an amorphous nature of SWP700, and crystalline Hg₂Cl₂ in Cl⁻ rich systems was not evident (Figure S5).

To further investigate the high Hg(II) removal in NaCl NOM systems, we compared the results to NaNO₃ at similar concentrations. In this case, even with the same amount of Na⁺ present in solution, Hg(II) removal was very low (K_d of 200 L kg⁻¹), proving that Cl⁻ drove Hg(II) removal in such systems. The presence of high NaCl concentrations allowed Hg(II)-chloro complexes to be formed over time, which were better immobilized than Hg-NOM species. The binding energies of Hg(II) with ligands follow the order of reactive S (log $K \sim 21$ -47) > Cl⁻ as HgCl₂, HgCl₃¹⁻, or HgCl₄²⁻ (log $K \sim 14$ -15.54) > O²⁻ as Hg-COO⁻ (log $K \sim 7.3$ -11).⁴⁹ Thus, Hg(II)

may have sorbed via a stepwise mechanism of ligand exchange followed by immobilization to the biochar surface: Cl^- competed with weakly bound O in NOM for Hg(II) complexation, forming Hg(II) -chloro complexes.⁵² These Hg(II) -chloro complexes having a smaller size than Hg-NOM could probably better access the porous structure of SWP700. Stronger binding reactive S groups within this porous framework could further competitively displace Cl^- (eqs 6 and 7).



The presence of Hg(II) as Hg(II) complexed to S on SWP700 was confirmed by EXAFS spectroscopy, where shell-by-shell fitting of the experimental spectrum yielded 1.8(0.1) S atoms neighboring Hg(II) at 2.32(0.03) Å on SWP700 (Figure S10). This coordination environment is similar to that which has been observed for Hg(II) bound to reactive S or thiol groups.^{53,54} Colocation of Hg(II) and S was further observed in μ -XRF mapping (25 μm beam size), although Cl^- and S were seen to be equally collocated with Hg(II) (Figure S7).

The importance of chloro-complexes in this Hg(II) removal mechanism by SWP700 was further confirmed through experiments conducted at a more acidic pH of 5.0 (Figure S13a). Even in the absence of Cl^- , systems at pH 5.0 showed higher Hg(II) removal than systems at pH 6.9 (K_d of 494 and 50 L kg^{-1} , respectively). This can be attributed to the decreased solubility of NOM and NOM complexed to Hg(II) at lower pH, which allowed more Hg(II) to be removed from solution.⁵⁵ At low pH, O groups tend to be protonated, which decreases the stability of Hg-NOM complexes.⁵⁶ Compared to higher pH scenarios, this enables Cl^- to more easily replace those groups as Hg(II) binding partner. As seen from WHAM VI calculations (Figure S13b), a large fraction of Hg(II) existed as HgCl_2 at pH 5.0 (83%) compared to pH 6.9 (5%). This facilitated more transfer of Hg(II) -chloro complexes to sorption sites within SWP700, at lower pH, which was in good agreement with the proposed stepwise sorption mechanism. Systems at lower pH saw an even larger surge in Hg(II) removal linked to the addition of NaCl: A 5.3-fold increase in K_d in a 5 mM Cl^- system, relative to a system without any Cl^- , was observed (from 494 to 2600 L kg^{-1}), followed by a further 1.7-fold increase in K_d when increasing Cl^- to 100 mM (from 2600 L kg^{-1} to 4430 L kg^{-1}).

In addition to Cl^- facilitating Hg(II) removal, high Hg(II) removal was also observed in Ca^{2+} -rich systems (Figure 4a). WHAM VI determined that 45–60% of Hg(II) in solution existed as Hg(II) -chloro complexes (Figure 4b). Fitting of the EXAFS spectrum to the 20 mM CaCl_2 sample yielded 2.2(0.2) S neighboring Hg(II) at a distance of 2.4(0.01) Å (Figure S9). Moreover, as seen in μ -XRF images (25 μm beam size), Hg(II) was correlated with S (Figure S7). Therefore, the mechanisms in eqs 6 and 7 would still dictate Hg(II) removal in the 20 mM CaCl_2 system. However, this did not fully explain the \sim 6.5-fold increase in K_d compared to the 100 mM NaCl system. Even 2.5 mM CaCl_2 significantly removed more Hg(II) than 5 mM NaCl.

In suspensions with Ca^{2+} , even at very low concentrations, strong NOM aggregation has been reported.⁵⁷ Ca^{2+} can associate multiple NOM molecules electrostatically or through

specific binding, increasing the hydrophobicity and aggregation of the supramolecular network of NOM. According to WHAM VI, the charge equivalents per mg of fulvic acids decreased from -5 (in solutions without ions) to -1.5 (in 20 mM CaCl_2 solutions). The ζ -potential in Ca^{2+} -NOM rich systems was in the range of -9 to -15 mV, which was significantly less negative than the range of -26 mV to -36 mV observed in Na^+ -NOM systems (Figure S3). This supports destabilization and increased hydrophobicity of NOM in Ca^{2+} -rich systems via cation bridging and charge-shielding effects. Simultaneously, we visually observed the formation of NOM aggregates and measured NOM removal up to 78% from solution at the end of experiments (Figure S4). Due to methodological limitations, it was not possible to distinguish between the truly sorbed and the NOM-coagulated fractions of Hg(II) . Aqueous phase recoveries in systems without biochar, though not completely transferrable to systems with biochar, were used to, in part, correct for this (Table S3). Additionally, EDS analysis of the surface of SWP700 showed that Ca^{2+} was present, unlike in pristine SWP700 (Figure S6). In this system, speciation results indicated that 40% of Hg(II) was associated with NOM (Figure 4b). Ca^{2+} therefore removed NOM, including NOM-bound Hg(II) from the aqueous phase. The high Hg(II) removal in CaCl_2 -NOM systems can be explained by a combination of chloro complex formation together with destabilization of NOM/ Hg(II) -NOM.

The importance of Ca^{2+} is further emphasized by the high Hg(II) and NOM removal observed in 20 mM $\text{Ca(NO}_3)_2$ systems, free of Cl^- (Figure 4a). In such systems, the mechanism of chloro complex-mediated Hg(II) removal would no longer be relevant. Although removal with $\text{Ca(NO}_3)_2$ was lower than in its CaCl_2 counterpart, it was still significantly higher than in 100 mM NaCl and 100 mM NaNO_3 . A clear peak of Ca^{2+} on SWP700's surface was also observed via EDS with 20 mM $\text{Ca(NO}_3)_2$ (Figure S6). EXAFS showed a distinct difference in the coordination environment compared to CaCl_2 and NaCl scenarios (Figure S8). Despite interferences due to beam damage (Figure S12), the peak at \sim 2.2 Å could only be fit with a Hg(I) - Hg(I) path (Figure S11). This may be explained by localized reducing environments close to the biochar surface, in line with previous propositions by others.^{10,13} Owing to SWP700's high pyrolysis temperature, its aromatic π -conjugated system was possibly the primary electron donating center for Hg(II) reduction to Hg(I) . This result further underlines the diversity in removal mechanisms for contaminants by biochars under different water chemistry conditions.

Implications for Industrial Water Treatment. This study elucidated that NOM, ionic composition, and pH are crucial drivers for Hg(II) removal from highly contaminated waters by a wood-based biochar. Hg(II) removal by biochar is generally suppressed in the presence of NOM. Our results show, however, that the ionic composition of contaminated waters has a strong influence on the removal efficiency and may lead to an effective clean-up even at higher NOM concentrations. Specifically, this will occur at high Cl^- concentrations where Cl^- can effectively displace O-containing moieties in NOM. Hg(II) removal in the presence of Cl^- followed a stepwise mechanism: weakly bound oxygen functional groups in NOM were outcompeted by Cl^- forming smaller-sized Hg(II) -chloro complexes. Cl^- was outcompeted by S groups in biochar which finally immobilized Hg(II) . Cations such as Ca^{2+} enhance Hg(II) removal through charge

shielding, cation bridging, and aggregation of Hg-NOM complexes.

These processes are dependent on the molar ratios of Hg(II)/NOM, Hg(II)/Cl, and NOM/Cl, as well as the pH. In lesser contaminated waters, low salinity organic matter rich waters, highly alkaline waters (pH > 9), or in waters containing a large fraction of reduced S, the observed effects might differ. This study did not investigate anoxic and sulfidic waste waters, where Hg(II) speciation and removal by biochar will differ.

■ ASSOCIATED CONTENT

SI Supporting Information

The Supporting Information is available free of charge at <https://pubs.acs.org/doi/10.1021/acs.est.2c01554>.

Preparation of NOM extract, WHAM VI speciation calculations, aqueous phase Hg(II) recovery in NOM containing background solutions, SWP700 bulk characterization, determination of total Hg using CVAFS, calculation of sorption coefficients (K_d), ζ -potential and pH measurements, removal of NOM, XRD and EDS measurements, generation of μ -XRF plots, EXAFS point selection and data processing, details on EXAFS fitting procedure, and effect of pH on Hg(II) removal in the presence of NOM (PDF)

■ AUTHOR INFORMATION

Corresponding Author

Thilo Hofmann – Department of Environmental Geosciences, Centre for Microbiology and Environmental Systems Science, University of Vienna, Vienna 1090, Austria; orcid.org/0000-0001-8929-6933; Phone: +43-1-4277-53320; Email: thilo.hofmann@univie.ac.at

Authors

Sampriti Chaudhuri – Department of Environmental Geosciences, Centre for Microbiology and Environmental Systems Science, University of Vienna, Vienna 1090, Austria; Doctoral School in Microbiology and Environmental Science, University of Vienna, Vienna 1090, Austria; orcid.org/0000-0002-8693-8758

Gabriel Sigmund – Department of Environmental Geosciences, Centre for Microbiology and Environmental Systems Science, University of Vienna, Vienna 1090, Austria; orcid.org/0000-0003-2068-0878

Sharon E. Bone – Stanford Synchrotron Radiation Lightsource, SLAC National Accelerator Laboratory, Menlo Park, California 94025, United States; orcid.org/0000-0002-7521-9627

Naresh Kumar – Soil Chemistry and Chemical Soil Quality Group, Wageningen University, Wageningen 6708 PB, The Netherlands; orcid.org/0000-0002-8593-5758

Complete contact information is available at: <https://pubs.acs.org/10.1021/acs.est.2c01554>

Notes

The authors declare no competing financial interest.

■ ACKNOWLEDGMENTS

This research was funded by the Austrian Federal Ministry for Climate Action, Environment, Energy, Mobility, Innovation and Technology (BMK) and managed by Kommunalkredit Public Consulting GmbH (grant number B820017). EXAFS at

the Stanford Synchrotron Radiation Lightsource, SLAC National Accelerator Laboratory is supported by the U.S. Department of Energy, Office of Science, Office of Basic Energy Sciences under Contract no. DE-AC02-76SF00515.

■ REFERENCES

- (1) Liu, G.; Cai, Y.; O'Driscoll, N.; Feng, X.; Jiang, G. Overview of Mercury in the Environment. *Environ. Chem. Toxicol. Mercury* **2011**, *18*, 1–12.
- (2) Gustin, M. S.; Evers, D. C.; Bank, M. S.; Hammerschmidt, C. R.; Pierce, A.; Basu, N.; Blum, J.; Bustamante, P.; Chen, C.; Driscoll, C. T.; Horvat, M.; Jaffe, D.; Pacyna, J.; Pirrone, N.; Selin, N. Importance of Integration and Implementation of Emerging and Future Mercury Research into the Minamata Convention. *Environ. Sci. Technol.* **2016**, *50*, 2767–2770.
- (3) Marrugo-Negrete, J.; Enamorado-Montes, G.; Durango-Hernández, J.; Pinedo-Hernández, J.; Díez, S. Removal of Mercury from Gold Mine Effluents Using *Limnorcharis Flava* in Constructed Wetlands. *Chemosphere* **2017**, *167*, 188–192.
- (4) Chen, H.; Zhan, L.; Gu, L.; Zhou, H.; Feng, Q.; Wu, H.; Zhao, S.; Yang, L. Fate and Distribution of Mercury during the Desulfurization Wastewater Evaporation Process. *Fuel* **2022**, *318*, 123609.
- (5) Clyde Vincent, J. A. Comparative Study of Heavy Metal Contamination at Common Biomedical Waste Treatment and Disposal Sites (Incineration and Deep Burial) in Mumbai, Maharashtra, India. -. *Int. J. Heal. Sci. Res.* **2016**, *6*, 415–419.
- (6) Sharma, P.; Iqbal, H. M. N.; Chandra, R. Evaluation of Pollution Parameters and Toxic Elements in Wastewater of Pulp and Paper Industries in India: A Case Study. *Case Stud. Chem. Environ. Eng.* **2022**, *5*, 100163.
- (7) Richard, J. H.; Bischoff, C.; Biester, H. Comparing Modeled and Measured Mercury Speciation in Contaminated Groundwater: Importance of Dissolved Organic Matter Composition. *Environ. Sci. Technol.* **2016**, *50*, 7508–7516.
- (8) Huang, Y.; Du, J. R.; Zhang, Y.; Lawless, D.; Feng, X. Removal of Mercury (II) from Wastewater by Polyvinylamine-Enhanced Ultrafiltration. *Sep. Purif. Technol.* **2015**, *154*, 1–10.
- (9) Wang, L.; Li, X.; Tsang, D. C. W.; Jin, F.; Hou, D. Green Remediation of Cd and Hg Contaminated Soil Using Humic Acid Modified Montmorillonite: Immobilization Performance under Accelerated Ageing Conditions. *J. Hazard. Mater.* **2020**, *387*, 122005.
- (10) Sánchez-Polo, M.; Rivera-Utrilla, J. Adsorbent–Adsorbate Interactions in the Adsorption of Cd(II) and Hg(II) on Ozonized Activated Carbons. *Environ. Sci. Technol.* **2002**, *36*, 3850–3854.
- (11) Bai, Y.; Hong, J. Preparation of a Novel Millet Straw Biochar-Bentonite Composite and Its Adsorption Property of Hg²⁺ in Aqueous Solution. *Materials* **2021**, *14*, 1117.
- (12) Dong, X.; Ma, L. Q.; Zhu, Y.; Li, Y.; Gu, B. Mechanistic Investigation of Mercury Sorption by Brazilian Pepper Biochars of Different Pyrolytic Temperatures Based on X-Ray Photoelectron Spectroscopy and Flow Calorimetry. *Environ. Sci. Technol.* **2013**, *47*, 12156–12164.
- (13) Xu, X.; Schierz, A.; Xu, N.; Cao, X. Comparison of the Characteristics and Mechanisms of Hg(II) Sorption by Biochars and Activated Carbon. *J. Colloid Interface Sci.* **2016**, *463*, 55–60.
- (14) Hsu, H.; Sedlak, D. L. Strong Hg(II) Complexation in Municipal Wastewater Effluent and Surface Waters. *Environ. Sci. Technol.* **2003**, *37*, 2743–2749.
- (15) Hudson, N.; Baker, A.; Reynolds, D. Fluorescence analysis of dissolved organic matter in natural, waste and polluted waters—a review. *River Res. Appl.* **2007**, *23*, 631–649.
- (16) Gai, K.; Avellan, A.; Hoelen, T. P.; Lopez-Linares, F.; Hatakeyama, E. S.; Lowry, G. V. Impact of Mercury Speciation on Its Removal from Water by Activated Carbon and Organoclay. *Water Res.* **2019**, *157*, 600–609.
- (17) Johs, A.; Eller, V. A.; Mehlhorn, T. L.; Brooks, S. C.; Harper, D. P.; Mayes, M. A.; Pierce, E. M.; Peterson, M. J. Dissolved Organic

Matter Reduces the Effectiveness of Sorbents for Mercury Removal. *Sci. Total Environ.* **2019**, *690*, 410–416.

(18) Bäckström, M.; Dario, M.Å.; Karlsson, S.; Allard, B. Effects of a Fulvic Acid on the Adsorption of Mercury and Cadmium on Goethite. *Sci. Total Environ.* **2003**, *304*, 257–268.

(19) Kelly, W. R.; Panno, S. V.; Hackley, K. *The Sources, Distribution, and Trends of Chloride in the Waters of Illinois*. Illinois State Water Survey Bulletin B, 2012; Vol. 1–59.

(20) Ravichandran, M. Interactions between mercury and dissolved organic matter—a review. *Chemosphere* **2004**, *55*, 319–331.

(21) Kim, C. S.; Rytuba, J. J.; Brown, G. E. EXAFS study of mercury(II) sorption to Fe- and Al-(hydr)oxides. *J. Colloid Interface Sci.* **2004**, *270*, 9–20.

(22) Cabaniss, S. E. Forward Modeling of Metal Complexation by NOM: II. Prediction of Binding Site Properties. *Environ. Sci. Technol.* **2011**, *45*, 3202–3209.

(23) Tan, Z.; Yuan, S.; Hong, M.; Zhang, L.; Huang, Q. Mechanism of Negative Surface Charge Formation on Biochar and Its Effect on the Fixation of Soil Cd. *J. Hazard. Mater.* **2020**, *384*, 121370.

(24) Koelmans, A. A.; Meulman, B.; Meijer, T.; Jonker, M. T. O. Attenuation of Polychlorinated Biphenyl Sorption to Charcoal by Humic Acids. *Environ. Sci. Technol.* **2009**, *43*, 736–742.

(25) Chen, M.; Wang, D.; Yang, F.; Xu, X.; Xu, N.; Cao, X. Transport and Retention of Biochar Nanoparticles in a Paddy Soil under Environmentally-Relevant Solution Chemistry Conditions. *Environ. Pollut.* **2017**, *230*, 540–549.

(26) Liang, X.; Lu, X.; Zhao, J.; Liang, L.; Zeng, E. Y.; Gu, B. Stepwise Reduction Approach Reveals Mercury Competitive Binding and Exchange Reactions within Natural Organic Matter and Mixed Organic Ligands. *Environ. Sci. Technol.* **2019**, *53*, 10685–10694.

(27) Salminen, R.; Batista, M. J.; Bidovec, M.; Demetriades, A.; De Vivo, B.; De Vos, W.; Duris, M.; Gilucis, A.; Gregorauskiene, V.; Halamić, J.; Heitzmann, P. Statistical Data of Analytical Results. *Geochemical Atlas Eur. Part 1, Backgr. Information, Methodol. Maps*, 2005.

(28) Jones, A. M.; Collins, R. N.; Rose, J.; Waite, T. D. The Effect of Silica and Natural Organic Matter on the Fe(II)-Catalysed Transformation and Reactivity of Fe(III) Minerals. *Geochim. Cosmochim. Acta* **2009**, *73*, 4409–4422.

(29) Bone, S. E.; Bargar, J. R.; Sposito, G. Mackinawite (FeS) Reduces Mercury(II) under Sulfidic Conditions. *Environ. Sci. Technol.* **2014**, *48*, 10681–10689.

(30) Zhong, D.; Ren, S.; Dong, X.; Yang, X.; Wang, L.; Chen, J.; Zhao, Z.; Zhang, Y.; Tsang, D. C. W.; Crittenden, J. C. Rice Husk-Derived Biochar Can Aggravate Arsenic Mobility in Ferrous-Rich Groundwater during Oxygenation. *Water Res.* **2021**, *200*, 117264.

(31) Strawn, D. G.; Sparks, D. L. Effects of Soil Organic Matter on the Kinetics and Mechanisms of Pb(II) Sorption and Desorption in Soil. *Soil Sci. Soc. Am. J.* **2000**, *64*, 144–156.

(32) Tipping, E. Modelling the Interactions of Hg(II) and Methylmercury with Humic Substances Using WHAM/Model VI. *Appl. Geochem.* **2007**, *22*, 1624–1635.

(33) Ippolito, J. A.; Cui, L.; Kammann, C.; Wrage-Mönnig, N.; Estavillo, J. M.; Fuertes-Mendizabal, T.; Cayuela, M. L.; Sigua, G.; Novak, J.; Spokas, K.; Borchard, N. Feedstock Choice, Pyrolysis Temperature and Type Influence Biochar Characteristics: A Comprehensive Meta-Data Analysis Review. *Biochar* **2020**, *2*, 421–438.

(34) Leng, L.; Liu, R.; Xu, S.; Mohamed, B. A.; Yang, Z.; Hu, Y.; Chen, J.; Zhao, S.; Wu, Z.; Peng, H.; Li, H.; Li, H. An Overview of Sulfur-Functional Groups in Biochar from Pyrolysis of Biomass. *J. Environ. Chem. Eng.* **2022**, *10*, 107185.

(35) Ravel, B.; Newville, M. ATHENA.; ARTEMIS, HEPHAESTUS. ATHENA, ARTEMIS, HEPHAESTUS: data analysis for X-ray absorption spectroscopy using IFEFFIT. *J. Synchrotron Radiat.* **2005**, *12*, 537–541.

(36) Liu, Z.; Dugan, B.; Masiello, C. A.; Gonnermann, H. M. Biochar Particle Size, Shape, and Porosity Act Together to Influence Soil Water Properties. *PLoS One* **2017**, *12*, No. e0179079.

(37) Srocke, F.; Han, L.; Dutilleul, P.; Xiao, X.; Smith, D. L.; Mašek, O. Synchrotron X-Ray Microtomography and Multifractal Analysis for the Characterization of Pore Structure and Distribution in Softwood Pellet Biochar. *Biochar* **2021**, *3*, 671–686.

(38) Wong, J. W. C.; Webber, J. B. W.; Ogbonnaya, U. O. Characteristics of Biochar Porosity by NMR and Study of Ammonium Ion Adsorption. *J. Anal. Appl. Pyrolysis* **2019**, *143*, 104687.

(39) Liu, P.; Ptacek, C. J.; Blowes, D. W.; Landis, R. C. Mechanisms of Mercury Removal by Biochars Produced from Different Feedstocks Determined Using X-Ray Absorption Spectroscopy. *J. Hazard. Mater.* **2016**, *308*, 233–242.

(40) Cheah, S.; Malone, S. C.; Feik, C. J. Speciation of Sulfur in Biochar Produced from Pyrolysis and Gasification of Oak and Corn Stover. *Environ. Sci. Technol.* **2014**, *48*, 8474–8480.

(41) Fabre, E.; Lopes, C. B.; Vale, C.; Pereira, E.; Silva, C. M. Valuation of Banana Peels as an Effective Biosorbent for Mercury Removal under Low Environmental Concentrations. *Sci. Total Environ.* **2020**, *709*, 135883.

(42) Tan, G.; Sun, W.; Xu, Y.; Wang, H.; Xu, N. Sorption of Mercury (II) and Atrazine by Biochar, Modified Biochars and Biochar Based Activated Carbon in Aqueous Solution. *Bioresour. Technol.* **2016**, *211*, 727–735.

(43) Yang, F.; Xu, Z.; Yu, L.; Gao, B.; Xu, X.; Zhao, L.; Cao, X. Kaolinite Enhances the Stability of the Dissolvable and Undissolvable Fractions of Biochar via Different Mechanisms. *Environ. Sci. Technol.* **2018**, *52*, 8321–8329.

(44) Li, H.; McKay, G. Relationships between the Physicochemical Properties of Dissolved Organic Matter and Its Reaction with Sodium Borohydride. *Environ. Sci. Technol.* **2021**, *55*, 10843–10851.

(45) Feng, Y.; Liu, P.; Wang, Y.; Liu, W.; Liu, Y. Y.; Finfrook, Y. Z. Mechanistic Investigation of Mercury Removal by Unmodified and Fe-Modified Biochars Based on Synchrotron-Based Methods. *Sci. Total Environ.* **2020**, *719*, 137435.

(46) Kwon, S.; Pignatello, J. J. Effect of Natural Organic Substances on the Surface and Adsorptive Properties of Environmental Black Carbon (Char): Pseudo Pore Blockage by Model Lipid Components and Its Implications for N₂-Probed Surface Properties of Natural Sorbents. *Environ. Sci. Technol.* **2005**, *39*, 7932–7939.

(47) Haitzer, M.; Aiken, G. R.; Ryan, J. N. Binding of Mercury(II) to Dissolved Organic Matter: The Role of the Mercury-to-DOM Concentration Ratio. *Environ. Sci. Technol.* **2002**, *36*, 3564–3570.

(48) Khwaja, A. R.; Bloom, P. R.; Brezonik, P. L. Binding Constants of Divalent Mercury (Hg²⁺) in Soil Humic Acids and Soil Organic Matter. *Environ. Sci. Technol.* **2006**, *40*, 844–849.

(49) Dong, W.; Liang, L.; Brooks, S.; Southworth, G.; Gu, B. Roles of Dissolved Organic Matter in the Speciation of Mercury and Methylmercury in a Contaminated Ecosystem in Oak Ridge, Tennessee. *Environ. Chem.* **2010**, *7*, 94.

(50) Lee, S.; Roh, Y.; Kim, K. W. Influence of Chloride Ions on the Reduction of Mercury Species in the Presence of Dissolved Organic Matter. *Environ. Geochem. Health* **2019**, *41*, 71–79.

(51) Si, L.; Ariya, P. A. Reduction of Oxidized Mercury Species by Dicarboxylic Acids (C₂–C₄): Kinetic and Product Studies. *Environ. Sci. Technol.* **2008**, *42*, 5150–5155.

(52) Song, Y.; Jiang, T.; Liem-Nguyen, V.; Sparrman, T.; Björn, E.; Skyllberg, U. Thermodynamics of Hg(II) Bonding to Thiol Groups in Suwannee River Natural Organic Matter Resolved by Competitive Ligand Exchange, Hg LIII-Edge EXAFS and ¹H NMR Spectroscopy. *Environ. Sci. Technol.* **2018**, *52*, 8292–8301.

(53) Manceau, A.; Lemouchi, C.; Rovezzi, M.; Lanson, M.; Glatzel, P.; Nagy, K. L.; Gautier-Luneau, I.; Joly, Y.; Enescu, M. Structure, Bonding, and Stability of Mercury Complexes with Thiolate and Thioether Ligands from High-Resolution XANES Spectroscopy and First-Principles Calculations. *Inorg. Chem.* **2015**, *54*, 11776–11791.

(54) Skyllberg, U.; Bloom, P. R.; Qian, J.; Lin, C. M.; Bleam, W. F. Complexation of Mercury(II) in Soil Organic Matter: EXAFS Evidence for Linear Two-Coordination with Reduced Sulfur Groups. *Environ. Sci. Technol.* **2006**, *40*, 4174–4180.

(55) Römken, P. F.; Bril, J.; Salomons, W. Interaction between Ca^{2+} and Dissolved Organic Carbon: Implications for Metal Mobilization. *Appl. Geochem.* **1996**, *11*, 109–115.

(56) Benoit, J. M.; Mason, R. P.; Gilmour, C. C.; Aiken, G. R. Constants for Mercury Binding by Dissolved Organic Matter Isolates from the Florida Everglades. *Geochim. Cosmochim. Acta* **2001**, *65*, 4445–4451.

(57) Wang, L. F.; Wang, L. L.; Ye, X. D.; Li, W. W.; Ren, X. M.; Sheng, G. P.; Yu, H. Q.; Wang, X. K. Coagulation Kinetics of Humic Aggregates in Mono- and Di-Valent Electrolyte Solutions. *Environ. Sci. Technol.* **2013**, *47*, 5042–5049.